A Fast Sinc Function Gridding Algorithm for Fourier Inversion in Computer Tomography

J. D. O'SULLIVAN

Abstract—**The Fourier inversion method for reconstruction of images in computerized tomography has not been widely used owing to the perceived difficulty of interpolating from polar or other measurement grids to the Cartesian grid required for fast numerical Fourier inversion. Although the Fourier inversion method is recognized as being computationally faster than the back-projection method for parallel ray projection data, the artifacts resulting from inaccurate interpolation have generally limited application of the method. This paper presents a computationally efficient gridding algorithm which can be used with direct Fourier transformation to achieve arbitrarily small artifact levels. The method has potential for application to other measurement geometries such as fan-beam projections and diffraction tomography and NMR imaging.**

I. Introduction

THE considerable numerical advantage of the Fourier inversion method over the filtered back-projection method is well known in the field of computer tomography [1]. In situations such as diffraction tomography the measurements are most naturally expressed in the Fourier domain and the comparison between the back-propagation algorithm of Devaney [2] and the direct Fourier reconstruction reveals even greater improvements in computational efficiency for the Fourier method [3].

Application of Fourier transform reconstruction methods is limited by the perceived difficulty of interpolation from the measured polar or other grid to the Cartesian grid required for efficient computation of the Fourier transform. Various interpolation schemes have been considered, such as nearest-neighbor, bilinear interpolation, and truncated sinc function FIR interpolators [3]–[5]. In all cases there is a tradeoff between the computational effort required for the interpolation and the level of artifacts in the final image produced by faulty interpolation.

An alternative procedure, first used on radio astronomical data by Brouw [6] and subsequently refined by others (e.g., [7]) offers both computational efficiency and negligible artifacts. This procedure is shown to provide a close approximation to the optimal sinc function interpolation while requiring a computational burden approximating that of bilinear interpolation.

The requirements for interpolation are first considered. It is demonstrated that, in the strictest sense of the word, interpolation is not necessary. That is, the values at grid points may be chosen such that the image is equal to the exact inverse transformation within some region. The values are not in general required to equal the actual Fourier domain values at grid points. Such an operation is referred to as gridding.

The optimal gridding method in the situation of interest is shown to be a convolution with a function whose transform is rectangular and band-limited (a sinc function), followed by sampling on to a Cartesian grid. The optimal convolution function is of infinite extent and would require a prohibitive computational burden. When the optimal convolution function is truncated and windowed, the performance of the function is sharply degraded.

An efficient computational implementation of the gridding operation is then considered and its application to practical tomographic reconstruction is demonstrated.

Finally, a detailed comparison of computational load is made between the gridding method proposed in a Fourier reconstruction algorithm and a filtered back-projection algorithm.

II. Ideal Band-Limited Interpolation

The theoretical basis of band-limited interpolation is well known but will be first considered to permit a clear comparison to be drawn with the requirements of a more general gridding process.

Consider a function $\mu(x, y)$, which represents, for example, the absorptivity of an object to be imaged. We assume first that $\mu(x, y)$ is of compact support and that $\mu(x, y)$ is to be reconstructed by Fourier inversion from samples of its transform $M(u_K, v_K)$, where

$$M(u, v) = \int_{-\infty}^{\infty} \int_{-\infty}^{\infty} \mu(x, y) \exp(j2\pi(ux + vy))\, dx\, dy. \tag{1}$$

Suppose we have a compact support such that

$$\mu(x, y) = 0, \qquad \text{for } |x| > x_0 \text{ or } |y| > y_0. \tag{2}$$

Let the sampling in the Fourier domain be represented by some sampling function $S(u, v)$

$$\mathfrak{M}(u, v) = M(u, v) \cdot S(u, v) \tag{3}$$

where

$$S(u, v) = \sum_k a_k\, \delta(u - u_k, v - v_k) \tag{4}$$

Manuscript received February 28, 1985; revised September 13, 1985.

The author is with the Division of Radiophysics, CSIRO, Sydney, Australia.

with the a_k present to allow arbitrary weight factors in the inversion. The inverse transform of $\mathfrak{M}(u, v)$ is given by

$$\boldsymbol{\mu}(x, y) = \mu(x, y) \circledast s(x, y) \tag{5}$$

where $s(x, y)$ is the inverse transform of $S(u, v)$.

Suppose the measurements are made on a Cartesian grid such that

$$S(u, v) = III(u/u_0, v/v_0) \tag{6}$$

where the function comb(u, v) is

$$\text{comb}(u, v) = \sum_i \sum_j \delta(u - i, v - j) \tag{7}$$

and δ is the Dirac delta function. The inverse transform of comb$(u/u_0, v/v_0)$ is given by

$$\begin{aligned} &FT^{-1}\{\text{comb}(u/u_0, v/v_0)\} \\ &\quad = \sum_i \sum_j \delta(x - i/u_0, y - j/v_0) \\ &\quad = u_0 v_0 \text{ comb}(xu_0, yv_0). \end{aligned} \tag{8}$$

The sampled inverse transform is related to the exact object function by the well-known alias phenomenon

$$\begin{aligned} \boldsymbol{\mu}(x, y) &= u_0 v_0 \, \mu(x, y) \circledast \text{comb}(xu_0, yv_0) \\ &= \sum_i \sum_j \mu(x - i/u_0, y - j/v_0). \end{aligned} \tag{9}$$

Ideal band-limited interpolation is possible provided the region of compact support of $\mu(x, y)$ is smaller than that defined by the repeated or aliased responses described by (9). That is,

$$\begin{aligned} x_0 &< 1/2u_0 \\ y_0 &< 1/2v_0. \end{aligned} \tag{10}$$

In order to see this, suppose that we select a function $c(x, y)$

$$\begin{aligned} c(x, y) &= 1 \quad |x| \le x_1 \quad \text{and} \quad |y| \le y_1 \\ &= 0 \quad |x| > x_1 \quad \text{or} \quad |y| > y_1. \end{aligned} \tag{11}$$

Then clearly,

$$\mu(x, y) = \boldsymbol{\mu}(x, y) \cdot c(x, y) \tag{12}$$

provided that

$$\begin{aligned} x_0 \le x_1 &< \frac{1}{u_0} - x_0 \\ y_0 \le y_1 &< \frac{1}{v_0} - y_0. \end{aligned} \tag{13}$$

In the Fourier domain, we have

$$M(u, v) = \mathfrak{M}(u, v) \circledast C(u, v) \tag{14}$$

where

$$C(u, v) = 4x_1 y_1 \cdot \text{sinc}(2x_1 u) \cdot \text{sinc}(2y_1 v). \tag{15}$$

The sinc function band-limited interpolation process is completed by resampling on to a new grid with spacing (u_1, v_1) as described by replacing (u_0, v_0) by (u_1, v_1) in (9), provided

$$\begin{aligned} x_0 &\le 1/2u_1 \\ y_0 &\le 1/2v_1. \end{aligned} \tag{16}$$

It is evident that exact interpolation on to a Cartesian grid is possible such that the inverse transform of the interpolated values matches the initial function $\mu(x, y)$ everywhere. The resampled or interpolated values exactly agree with the values taken by $M(u, v)$ at the resample points.

III. Gridding for Functions of Noncompact Support

At this point we can draw an important distinction between interpolation and the more general gridding process. The problem as phrased initially was to estimate $\mu(x, y)$ by direct Fourier inversion of $\mathfrak{M}(u, v)$, or in other words, to compute $\boldsymbol{\mu}(x, y)$. We now drop the requirement that $\boldsymbol{\mu}(x, y)$ be of limited support (2) and the related requirements of the sampling density (13) and seek instead to compute $\boldsymbol{\mu}(x, y)$ within the region $|x| < x_1$ and $|y| < y_1$. Hence, we consider the truncated function $\boldsymbol{\mu}_c$

$$\boldsymbol{\mu}_c(x, y) = \boldsymbol{\mu}(x, y) \cdot c(x, y) \tag{17}$$

which is obtained by convolution in the Fourier domain of $\mathfrak{M}(u, v)$ with $C(u, v)$ [cf. (14)]. $\boldsymbol{\mu}(x, y)$ is preserved by the convolution for $|x| < x_1$, $|y| < y_1$.

Again, the continuous function $\mathfrak{M}(u, v)$ may be sampled on a Cartesian grid with spacing (u_1, v_1)

$$\begin{aligned} \mathfrak{M}_{cs}(u, v) &= \mathfrak{M}_c(u, v) \cdot \text{comb}(u/u_1, v/v_1) \\ &= [\mathfrak{M}(u, v) \circledast C(u, v)] \cdot \text{comb}(u/u_1, v/v_1) \end{aligned} \tag{18}$$

and again, as for (9) we obtain

$$\boldsymbol{\mu}_{cs}(x, y) = \sum_i \sum_j \boldsymbol{\mu}_c(x - i/u_1, y - j/v_1). \tag{19}$$

If the region of compact support of $\boldsymbol{\mu}_c(x, y)$ is smaller than the region defined by the repeated responses, then $\boldsymbol{\mu}_{cs}(x, y)$ is an accurate representation of $\boldsymbol{\mu}_c(x, y)$. That is, if we have

$$\begin{aligned} x_1 &\le 1/2u_1 \\ y_1 &\le 1/2v_1. \end{aligned} \tag{20}$$

The operation described by (18) is not an exact interpolation in general and will be referred to as a gridding operation. We define gridding then as a sinc function convolution and consequent sampling on a regular grid. In the case of inadequate or non-Cartesian sampling, or of lack of compact support of $\mu(x, y)$, or of both, the gridding operation is a method to produce a set of samples on a Cartesian grid such that the inverse Fourier transform of the gridded data is equal to that of the original sampled data within some region of the image domain. The grid-

ded values are not in general equal to the values of the original transform, even at the measured points.

There is no requirement on the density of samples in the Fourier domain, nor is there a requirement on the support of the object function $\mu(x, y)$. The sinc function gridding operation is appropriate when an inverse Fourier transform is required of samples on a nonuniform grid of measured points.

IV. Fast Sinc Function Gridding

The convolution of the sampled Fourier domain data with a sinc function followed by resampling and discrete inverse Fourier transformation has been demonstrated to be identical to direct Fourier inversion within some region of the image and solves the problem of gridding data measured or obtained on a nonuniformly spaced grid. The sinc function is of infinite extent, so each Fourier domain measurement generates contributions for all grid points in the Fourier domain and the solution as described is impractical.

Restriction of the convolution function $C(u, v)$ to a finite area of the Fourier domain necessarily requires $c(x, y)$ to be of infinite extent. Given that the object function $\boldsymbol{\mu}(x, y)$ is of infinite extent, as is necessitated by the finite sampling of $\mathfrak{M}(u, v)$ in the measurement process, then the product $\boldsymbol{\mu}_c(x, y)$ is also of infinite extent and the aliasing described by (19) produces errors or artifacts in the estimate of $\boldsymbol{\mu}_c(x, y)$. We see, however, from (17) and (19) that the object may be estimated by

$$\boldsymbol{\mu}_e(x, y) = \boldsymbol{\mu}_{cs}(x, y)/c(x, y), \qquad |x| < x_1, |y| < y_1 \quad (21)$$

where the restriction that $c(x, y)$ be constant within some domain of interest has been relaxed.

The central term $(i, j) = (0, 0)$ in the summation of (19) is corrected for the influence of $c(x, y)$ exactly. The error of the estimate μ_e is accordingly

$$\boldsymbol{\mu}_e(x, y) - \boldsymbol{\mu}(x, y) = \frac{1}{u_0 v_0} \sum_{i \neq 0} \sum_{j \neq 0} \boldsymbol{\mu}(x - i/u_0, y - j/v_0) \times c(x - i/u_0, y - j/v_0)/c(x, y). \quad (22)$$

The situation is shown in Fig. 1, where the sequence of convolution and sampling or gridding is portrayed in the image domain. The success of the method clearly lies in the rate of decay of $c(x, y)$ for $|x| > x_1$, $|y| > y_1$ compared to the values within the region. Schwab [7] defines an optimality criterion R

$$R = \frac{\int \int_A |c(x, y)|^2 \, w(x, y) \, dx \, dy}{\int_{-\infty}^{\infty} \int_{-\infty}^{\infty} |c(x, y)|^2 \, w(x, y) \, dx \, dy} \quad (23)$$

where A is the domain within which $c(x, y)$ is to be concentrated, and $w(x, y)$ is some weight function. He shows that for separable weight functions of the form $w(x, y) = (1 - x)^{\alpha} (1 - y)^{\alpha}$, R is maximized by a choice of $C(x, y) = C_x(x) C_y(y)$ (also separable), which can be represented in terms of zero-order prolate spheroidal wavefunctions [8].

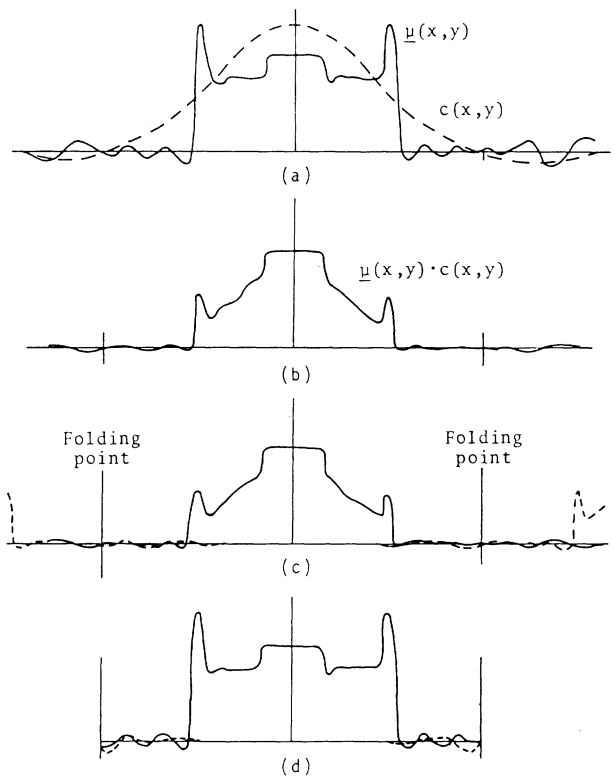

Fig. 1. Illustration of the operation of the convolution gridding method in the image or inverse transform domain. (a) Inverse transform $\boldsymbol{\mu}(x, y)$ (solid) of some measured $\mathfrak{M}(u, v)$ and the convolution function inverse transform $c(x, y)$. (b) After convolution in the Fourier domain, the result is equal to $\mu(x, y)\, c(x, y)$. (c) Sampling on to the Cartesian grid in the Fourier domain results in aliasing or folding of the spectrum. (d) Convolution correction by division with $c(x, y)$. The dotted component represents the error introduced by gridding.

The prolate spheroidal wavefunctions are difficult to compute accurately but a simple approximation is provided by the Kaiser–Bessel window function [9] defined by

$$C_x(u) = \frac{1}{L} I_0 \left[B(1 - (2u/L)^2)^{1/2}\right], \qquad u < L/2 \quad (24)$$

where I_0 is the zero-order modified Bessel function of the first kind and B and L are constants. The inverse transform is given by

$$c_x(x) = \frac{\sin (\pi^2 L^2 x^2 - B^2)^{1/2}}{(\pi^2 L^2 x^2 - B^2)^{1/2}}. \quad (25)$$

The parameter B, along with the extent of the window L, determines the characteristics of the window and its inverse transform. Selecting $c(x, y) = c_x(x) \cdot c_y(y)$ and somewhat arbitrarily choosing the parameter B as

$$B_x = \pi L_x x_1$$
$$B_y = \pi L_y y_1 \quad (26)$$

then $c(x)$ reaches the first null at $|x| = (x_1^2 + 1/L^2)^{1/2}$ and $|y| = (y_1^2 + 1/L^2)^{1/2}$. The inverse Fourier transform op-

eration will be performed with an $N_x \times N_y$ point discrete Fourier transform such that the points $|x| = x_1$ and $|y| = y_1$ are the folding points for the transform. We obtain, therefore, also $x_1 = 1/2u_0$, $y_1 = 1/2v_0$, and taking the convolution functions $c_x(x)$ and $c_y(y)$ to cover L_x, L_y points in the Fourier domain, we have

$$B_x = \pi L_x/2$$

$$B_y = \pi L_y/2 \tag{27}$$

where the grid interval in the Fourier domain is unity. Fig. 2 shows the Kaiser–Bessel window function and its transform for representative values of the window function extent L. As expected, the performance of the function as measured by rejection beyond the folding frequency is improved as L increases.

The effectiveness of this choice of convolution function can be shown for the case where $\mathfrak{M}(u, v)$ consists of a single sample. The inverse transform becomes of infinite extent and exhibits no decay. The convolution function is alone required to suppress artifacts due to aliasing. Fig. 3 shows the error for a single sample situated midway between two grid points in the Fourier domain. The error was computed by comparing a direct computation of the inverse Fourier transform using the exact measurement coordinate to a computation using the Kaiser–Bessel convolution function to perform gridding. A convolution function covering four grid points was employed. As expected, the errors become large near the folding points but the central half of the range yields errors less than 0.61 percent.

The central region may be retained and the outer region cleared or ignored. In the former case it can be seen that a good approximation to sinc function interpolation has been obtained with a convolution function of very limited extent. It may also be noted that the case considered is extreme. Any realistic set of measurements will exhibit a reduction in $\mu(x, y)$ for x, y large, thereby further reducing aliasing and the errors experienced.

The errors have been computed for the central region $|x| < x_1/2$, $|y| < y_1/2$ for a variety of situations and are shown in Table I for two representative cases. Coordinate $u = 10.5$ corresponds to the single sample midway between two grid points while $u = 10.001$ corresponds to the single sample lying very near a grid point. The errors increase somewhat for the latter case. The magnitude of the error is not strongly influenced since u is varied over a wide range but is found to increase when the convolution function overlaps the origin.

Evidently, the Kaiser–Bessel convolution function used with modest widths of 4 to 6 points corresponding to 16 to 36 points in two dimensions is capable of producing negligible artifacts. It may be noted that little effort has been devoted here to optimizing the parameters such as B and some additional improvements may be obtained in specific cases.

The practical sinc function approximation algorithm can be summarized as follows.

1) Convolve and grid the measured Fourier domain samples with a convolution function such as the Kaiser–Bessel window function. The kth sample produces a contribution to the surrounding grid points according to

$$\mathfrak{M}_{csk}(i + u, j + v) = a_k \mathfrak{M}(u_k, v_k)\, C(u_k - i - u, v_k - j - v), \quad -L_x \le i \le L_x, \quad -L_y \le j \le L_y \tag{28}$$

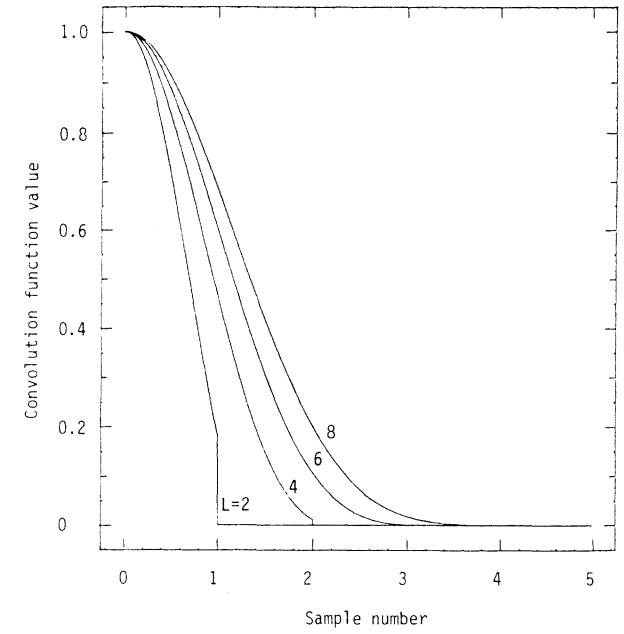

(a)

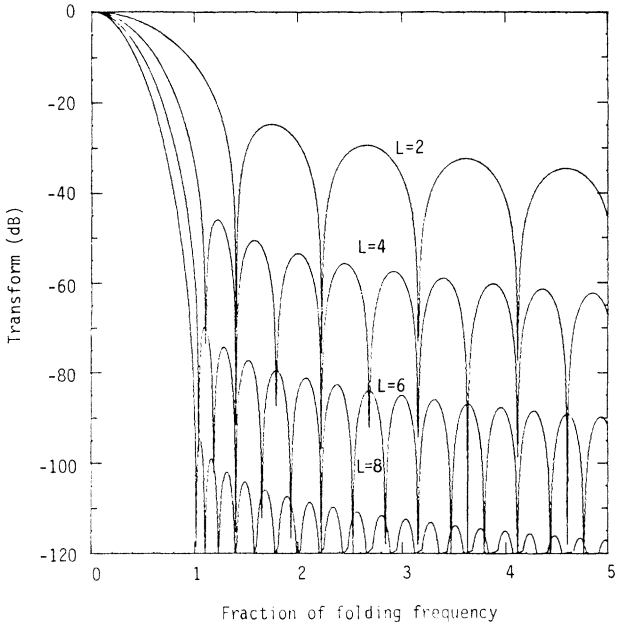

(b)

Fig. 2. (a) The Kaiser–Bessel convolution function for values of extent L = 2, 4, 6, 8. The horizontal axis is in units of the Cartesian grid for regridding. (b) The Fourier transform of the convolution functions of (a). The horizontal axis is in units of the discrete Fourier transform folding frequency.

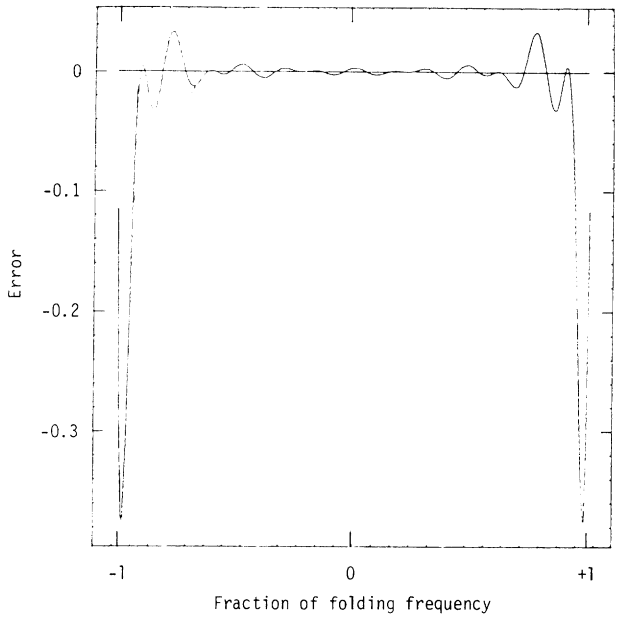

Fig. 3. Relative error in the inverse transform domain when the transform data consist of a single point in one dimension at $u = 10.5$. The inverse transform computed with the convolution gridding method using a 256-point complex to 512-point real transform is compared to the analytic inverse transform. A 4-point convolution function was used. In the central half of the inverse transform (-127 to 128) the error is found to be 0.6 percent peak or 0.28 percent rms.

where (u, v) is the nearest integer (grid point) such that $u < u_k$, $v < v_k$.

2) Inverse transform the gridded data to the image domain.

3) Correct for the effects of the convolution by dividing by $c(x, y)$ within the region of interest. Outside the region the image may be ignored or multiplied by zero. The latter produces a result equivalent to sinc function convolution.

The restriction of the domain of interest to the inner quarter (in two dimensions) of the transformed field means that effectively a $2N_x \times 2N_y$ transform must be computed to inverse transform to an acceptable $N_x \times N_y$ image.

V. Application to Parallel-Ray Projection and Diffraction Tomography

The application of direct Fourier reconstruction methods to parallel-ray projection data has been extensively considered in [1], [4], [5]. We present here only sufficient background to allow comparison of the interpolation technique above with the filtered back-projection algorithms in common use.

The measurements consist of samples of the line integral $p(s, \theta)$ of $\mu(x, y)$ along a line distance s from the origin and at angle θ. For parallel-ray projection geometry, a set of measurements for constant θ is taken and two reconstruction formulas are readily obtained [1].

The data may be transformed with respect to s to give $P(R, \theta)$, from which the direct Fourier reconstruction formula yields

TABLE I
Fractional Error in Central Region for Kaiser-Bessel Convolution

Exact coordinate = 10.5		
No. of points	Max error	RMS error
2	0.062	0.033
4	0.0061	0.0028
6	0.0003	0.00009
8	0.00003	0.000009
10	0.000003	0.0000001

Exact coordinate = 10.001		
No. of points	Max error	RMS err
2	0.171	0.102
4	0.015	0.00[illegible]
6	0.0006	0.00[illegible]
8	0.00003	0.00[illegible]
10	0.000002	0.00[illegible]

$$P(R, \theta) = \int_{-\infty}^{\infty} p(s, \theta)\, e^{j2\pi Rs}\, ds$$

$$\mu(x, y) = \int_0^{\pi} \int_{-\infty}^{\infty} P(R, \theta)\, e^{j2\pi R(x \cos\theta + y \sin\theta)} \cdot W(R)\, |R|\, dR\, d\theta \tag{29}$$

or the corresponding formulas with integration replaced by summation if $P(R, \theta)$ or $p(s, \theta)$ is sampled.

The alternative involves interchanging the integrals over R and s to obtain,

$$\mathcal{P}(s', \theta) = \int_{-\infty}^{\infty} p(s, \theta) \left[\int_{-\infty}^{\infty} |R| \; W(R) \; e^{j2\pi R(s'-s)} \, dR \right] ds$$

$$\mu(x, y) = \int_{0}^{\pi} \mathcal{P}(x \cos\theta + y \sin\theta, \theta) \, d\theta. \tag{30}$$

The intermediate quantity corresponds to a filtered or convolved projection, while the second operation is the back-projection. In practice, the filtering operation will be most efficiently performed by multiplication in the transform domain of the image size and the filter function are large so the first operations are equivalent in both methods.

Fig. 4(a) shows a phantom identical to that used in [3] as reconstructed with a back-projection algorithm using 64 projections. The reconstruction is 128 × 128 pixels. Fig. 4(b) shows the same data reconstructed with the approximate sinc function interpolation of this paper. A 4 × 4 Kaiser–Bessel convolution function was employed. The differences between the reconstructions are everywhere less than 0.15 percent of the peak value (0.05 percent rms). Increasing the convolution function to 6 × 6 extent reduced the errors to 0.02 percent peak (0.003 percent rms).

Stark *et al.* [4], [5] have employed various band-limited interpolation approximations to compute the direct Fourier inversion of parallel ray projection data. The best result was obtained with a convolutional filter of extent 5 × 3 polar points [5] which would involve comparable computation to the 4 × 4 point convolution above. The resulting performance for the algorithm of Stark *et al.* is not directly quantified but may be inferred from [5, Fig. 21] where a comparison to the filtered back projection reconstruction yields peak errors of order 10 percent.

To illustrate the fact that the method proposed here does not require an object of limited support, the central portion only of Fig. 4(b) was computed by gridding and Fourier inversion. The error over the common points is 0.04 percent peak and 0.01 percent rms.

The computational advantages of the method may be quantified by consideration of an inversion involving N_p projections on to N_i^2 pixels. The operation counts for each phase of the inversion methods will be compared. Each of the following subsections is represented by a box in Fig. 4.

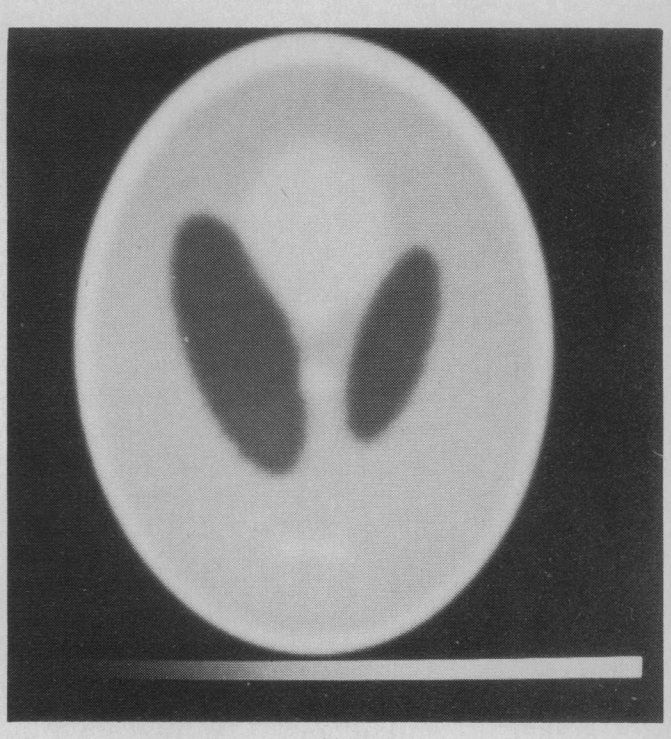

(a)

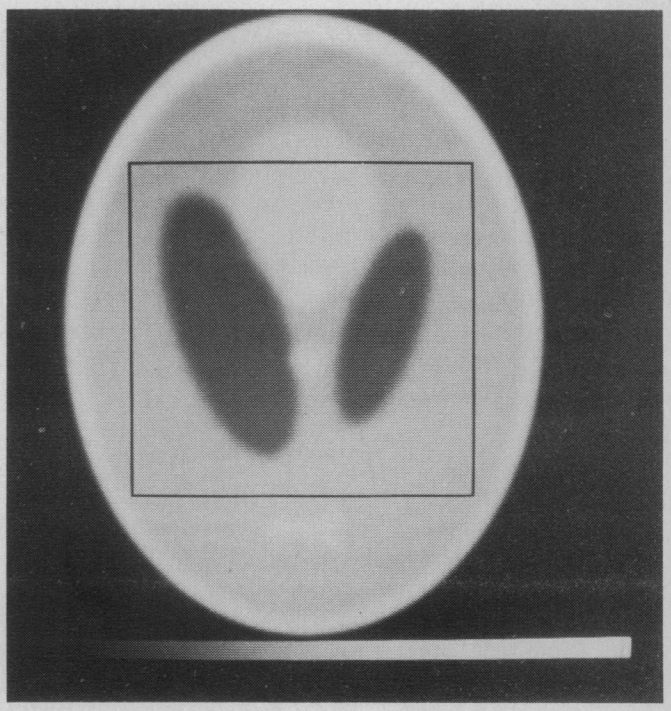

(b)

Fig. 4. Reconstructions of parallel ray projection data with 64 projections calculated according to the phantom of Pan and Kak [3]. (a) Back-projection algorithm with 128 × 128 pixels. (b) Fourier method using 4 × 4 convolution function and 128 × 128 pixels. Superimposed on the central quarter of the image is a Fourier reconstruction of the central portion alone, illustrating the success of the method even when the object is not of compact support.

A. Filtering Per Projection (Fourier and Back-Projection)

Equations (29) and (30) (assuming the filtering operation is performed in the Fourier domain) indicate that the first integral in the back-projection and direct Fourier inversion methods are identical and are therefore subject to the same requirements regarding number of points, etc. Roughly, we require a transform to $K_u N_i$ points, where K_u is of order 3–5 and is determined by the increment in the radial Fourier domain required to keep aliased responses out of the filtered projection or the image. We have then

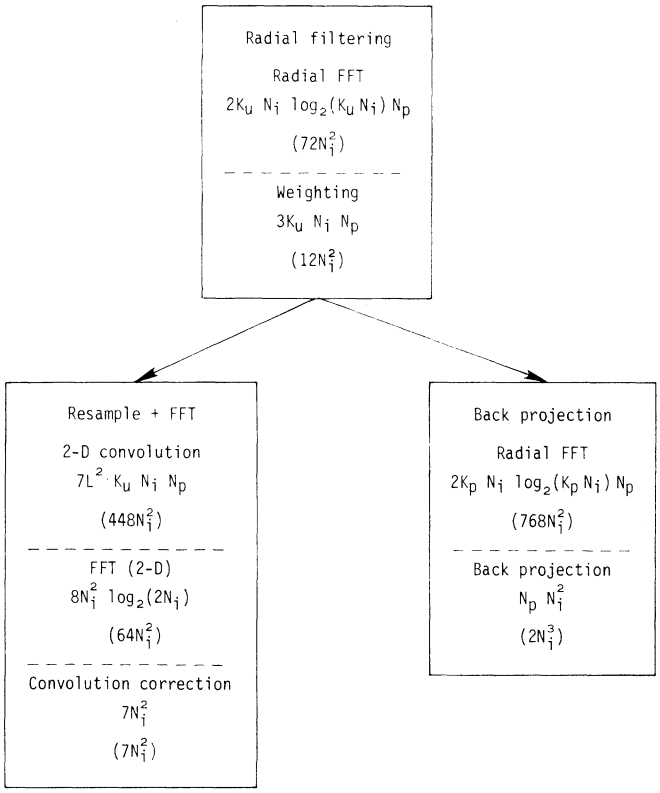

Fig. 5. Comparison of the multiplication operation counts for the various phases of the Fourier inversion and back-projection methods. The approximate figures (in brackets) are computed for $K_u = 4$, $K_p = 32$, $L = 4$, $N_p = N_i$, $\log_2(N_i) = 7$.

for both methods a radial transform contribution of $2K_uN_i \log_2(K_uN_i) N_p$ multiplications. Both methods require weighting by the factor $W(R) \cdot |R|$, which should require of order $3K_uN_iN_p$, operations where it is assumed that the composite weight factor is precomputed and tabulated and the overhead in linear interpolation and indexing is equivalent to three multiplications.

B. Inverse Radial Transformation (Back-Projection)

At this point the algorithms diverge. The back-projection algorithm requires inverse transformation to produce $\mathcal{P}(s, \theta)$. Assuming a simple linear interpolation algorithm is used in the back-projection phase, the number of points per resolution interval must be raised to greater than 10 points (however, other choices are possible). This might be achieved by zero-padding the inverse transform to give a total number of filtered projection points given by K_pN_i where K_p is 30–50. The inverse transform requires $2K_pN_i \log_2(K_pN_i) N_p$ operations.

C. Kaiser–Bessel Convolution (Fourier)

The comparable operation in the Fourier method is the Kaiser–Bessel convolution. Since we have $K_iN_iN_p$ points, with each requiring a convolution involving L^2 adjacent grid points the number of operations is of order $7L^2 K_uN_i N_p$, where it is assumed that the overhead in interpolating a tabulated convolution function table is three multiplications in each dimension.

D. Back-Projection

The back-projection operation requires an interpolation/table lookup per projection to be repeated for N_i^2 pixels. Assuming a minimal interpolation and indexing overhead of (2–3) multiplications, we obtain a total operation count for the back-projection operation of (2–3) $N_pN_i^2$.

E. Inverse Fourier Transform and Convolution Correction

The corresponding operation in the Fourier method is the fast Fourier transform (FFT) and correction for the Kaiser–Bessel convolution. Assuming that the transform must be over-dimensioned by a factor 2 in each coordinate, we obtain for the transform $8N_i^2 \log_2(2N_i)$ operations and approximately $7N_i^2$ for the convolution correction.

Improvements can be obtained by use of suitable real to complex and complex to real FFT algorithms where appropriate. The above calculations have been based on complex to complex transforms throughout for simplicity.

Fig. 5 provides a convenient summary of the multiplication counts involved in the various phases of each method. The dominant phases are the 2-D convolution in the Fourier method and the radial FFT and back-projection for the back-projection method. All operations except the back-projection operation are $O(N_i^2)$ whereas the latter is an $O(N_i^3)$ operation if $N_p \simeq N_i$. As size of images is increased to 512 × 512 and beyond, the back-projection operation will become the dominant factor. It may also be

noted that direct algorithms for the filter phase of the back-projection are also $O(N_i^3)$ operations.

The diffraction tomography case presents an even more extreme difference. Diffraction tomography can be shown [2], [3] in the case of the Born or Rytov approximations to yield measurements the transform of which lie not on radial lines in the Fourier domain but on circular arcs intersecting at the origin. The Fourier inversion is essentially unaffected in terms of operation count. The symmetry which allows the back-projection algorithm is, however, removed. Devaney [2] has introduced the back-propagation algorithm which is related to the back-projection algorithm but in which the filter operation must be applied with differing kernels for differing regions of the image. The filter operations become more intensive by a factor proportional to N_i such that in practical situations the filter operation will become the dominant part of the back-propagation algorithm.

VI. Conclusions

A fast sinc convolution algorithm for the gridding operation of the direct Fourier inversion of tomographic data has been presented. The algorithm allows the computational benefits of the direct Fourier inversion methods without incurring a significantly increased level of artifacts.

To some extent the deficiencies of the $O(N_i^3)$ back-projection algorithm are overcome in practical scanners by the use of high-speed, special-purpose hardware. The nature of the increase with image size means however that significant parallelism must be introduced to maintain the almost "direct" response time desired as image size is increased beyond 250^2 to 512^2 pixels. For larger images it is important to utilize the economies of efficient FFT methods wherever possible.

The NMR imaging modality [10] results in images containing large numbers of pixels and allows measurements to be made directly in the Fourier domain. The algorithm described could be particularly effective for NMR image reconstruction.

A further consideration is the potential use of reasonable reconstruction algorithms to allow high-quality imaging even in the face of limited angular coverage or number of projections. Algorithms such as the Gerchberg–Papoulis algorithm [11], [12] are of an iterative nature and require fast, efficient transformation and inverse transformation algorithms.

Acknowledgment

D. J. McLean provided valuable comments on earlier versions of this paper. The author also wishes to acknowledge useful comments and suggestions made by the referees.

References

[1] R. M. Lewitt, "Reconstruction algorithms: Transform methods," *Proc. IEEE*, vol. 71, no. 3, pp. 390–408, 1983.

[2] A. J. Devaney, "A filtered backpropagation algorithm for diffraction tomography," *Ultrason. Imaging*, no. 4, pp. 336–350, 1982.

[3] S. X. Pan and A. C. Kak, "A computational study of reconstruction algorithms for diffraction tomography: Interpolation versus filtered backpropagation," *IEEE Trans. Acoust., Speech, Signal Processing*, vol. ASSP-31, no. 5, pp. 1262–1275, 1983.

[4] H. Stark *et al.*, "Direct Fourier reconstruction in computer tomography," *IEEE Trans. Acoust., Speech, Signal Processing*, vol. ASSP-29, no. 2, pp. 237–245, 1981.

[5] ——, "An investigation of computerised tomography by direct Fourier inversion and optimum interpolation," *IEEE Trans. Biomed. Eng.*, vol. BME-28, no. 7, pp. 496–505, 1981.

[6] W. N. Brouw, "Aperture synthesis," in *Methods in Computational Physics*, no. 14. New York: Academic, 1975, pp. 131–175.

[7] F. R. Schwab, "Optimal gridding of visibility data in radio interferometry," in *Indirect Imaging*, J. A. Robers, Ed. New York: Cambridge University Press, 1983.

[8] D. Slepian and H. O. Pollack, "Prolate spheroidal wavefunctions, Fourier analysis and uncertainty—I," *Bell Syst. Tech. J.*, vol. 43, pp. 43–63, 1961.

[9] A. H. Nuttal, "Some windows with very good sidelobe behavior," *IEEE Trans. Acoust., Speech, Signal Processing.*, vol. ASSP-29, no. 1, pp. 84–91, 1981.

[10] W. S. Hinshaw and A. H. Lent, "An introduction to NMR imaging: From the block equation to the imaging equation," *Proc. IEEE*, vol. 71, no. 3, pp. 338–350, 1983.

[11] R. W. Gerchberg, "Super resolution through error energy reduction," *Opt. Acta*, vol. 21, pp. 709–720, 1974.

[12] A. Papoulis, "A new algorithm in spectral analysis and band limited extrapolation," *IEEE Trans. Circuits Syst.*, vol. CAS-22, pp. 753–742, 1975.